

# Hilda collisional family affected by planetary migration?

M. Brož<sup>1\*</sup>, D. Vokrouhlický<sup>1</sup>, A. Morbidelli<sup>2</sup>, W.F. Bottke<sup>3</sup>, D. Nesvorný<sup>3</sup>

<sup>1</sup>*Institute of Astronomy, Charles University, Prague, V Holešovičkách 2, 18000 Prague 8, Czech Republic*

<sup>2</sup>*Observatoire de la Côte d’Azur, BP 4229, 06304 Nice Cedex 4, France*

<sup>3</sup>*Department of Space Studies, Southwest Research Institute, 1050 Walnut St., Suite 300, Boulder, CO 80302, USA*

Accepted ???. Received ???; in original form ???

## ABSTRACT

We model a long-term evolution of the Hilda collisional family located in the 3/2 mean-motion resonance with Jupiter. It might be driven by planetary migration and later on by the Yarkovsky/YORP effect. Assuming that: (i) impact disruption was isotropic, and (ii) albedo distribution of small asteroids is the same as for large ones, we need at least a slight perturbation by planetary migration to explain the current large spread of the family in eccentricity. Hilda is thus the first family in the Main Belt, which may serve as a direct test of planetary migration. We tested a number of scenarios for the evolution of planetary orbits. We select those which perturb the Hilda family sufficiently (by secondary resonances) and, on the other hand, do not destroy the Hilda family completely. There is a preference for fast migration time scales  $\simeq 0.3$  Myr to 30 Myr at most and an indication, that Jupiter and Saturn were not in a compact configuration ( $P_J/P_S > 2.09$ ) at the time when the Hilda family had been created.

We also estimate collisional activity in the J3/2 region. Our results indicate that disruption frequencies are very low and one can expect an existence of at most one family with a 200 km parent body. More frequent collisions may be expected during planetary migration period, which is in agreement with the dynamical results.

**Key words:** celestial mechanics – minor planets, asteroids – methods:  $N$ -body simulations.

## 1 INTRODUCTION

There are many independent lines of evidence, that orbits of planets in the Solar System were not the same all the time, but that they have changed substantially over millennia. The arguments are based on the observed high eccentricities and inclinations of giant planets (Tsiganis et al. 2005), the amplitudes of secular oscillations (Brasser et al. 2010), orbital distribution of Jupiters Trojans (Morbidelli et al. 2005), Main-Belt asteroids (Minton & Malhotra 2009, Morbidelli et al. 2010) Kuiper belt objects (Malhotra et al. 1995) or the existence of irregular moons (Nesvorný et al. 2007).

Asteroids are definitely an important source of information about the evolution of the planetary system. Some of the resonant groups, i.e., located in the major mean-motion resonances with Jupiter, might have been also influenced by planetary migration, because their current distribution does not correspond to the current extent of stable orbits (Roig & Ferraz-Mello 1999).

In this work we focus on asteroid families *in resonances*.

We exploit our ability to model long-term evolution of asteroid families, which is usually dominated by the Yarkovsky drift in semimajor axis (Bottke et al. 2001), often coupled to the YORP effect affecting spin rate and obliquity (Vokrouhlický et al. 2006b). Chaotic diffusion in eccentricity and sometimes interactions with weak mean-motion or secular resonances (Vokrouhlický et al. 2006a) also play important roles. In case of asteroids inside strong mean-motion resonances, one has to account for the “resonant” *Yarkovsky effect*, which causes a systematic drift in eccentricity (Brož & Vokrouhlický 2008).

A Hilda collisional family — a part of the so called Hilda group in the 3/2 mean motion resonance with Jupiter — was already briefly discussed by Brož & Vokrouhlický (2008). The modelling presented in that paper was not very successful, thought, since the resulting age of the family seemed to be a bit too large (exceeding 4 Gyr). Today, we think we missed an important mechanism in our model, namely perturbations arising from migration of planets. Indeed, the age  $\gtrsim 4$  Gyr suggests, the planetary migration might have played a *direct* role during the early evolution of the Hilda family. In this paper we thoroughly test this hypothesis.

The paper is organised as follows: at first, we study

\* E-mail: mira@sirrah.troja.mff.cuni.cz

the observed properties of the J3/2 resonance population in Section 2. Our dynamical model of the Hilda family is described in Section 3. The results of our simulations are presented in Section 4 and 5 and finally, Section 6 is devoted to conclusions.

## 2 CURRENT ASTEROID POPULATION IN THE J3/2 RESONANCE

Our identification procedure of the J3/2 resonant population was described in the previous paper Brož and Vokrouhlický (2008). Using the AstOrb catalogue of orbits (version  $JD = 2455000.5$ , Jun 18th 2009) we identified 1534 bodies with librating critical argument

$$\sigma = \frac{p+q}{q}\lambda' - \frac{p}{q}\lambda - \varpi, \quad (1)$$

where  $p = 2$ ,  $q = 1$ ,  $\lambda'$  is the mean longitude of Jupiter,  $\lambda$  the mean longitude of the asteroid, and  $\varpi$  the longitude of perihelion of the asteroid.

In order to study detailed distribution of bodies librating inside the resonance we have to use pseudo-proper resonant elements defined as approximate surfaces of sections (Roig et al. 2002)

$$|\sigma| < 5^\circ, \quad \frac{\Delta\sigma}{\Delta t} > 0, \quad |\varpi - \varpi'| < 5^\circ. \quad (2)$$

These conditions correspond to a maximum of semimajor axis  $a$  over several oscillations and a minimum of eccentricity  $e$  or inclination  $I$ . We are forced to apply a digital filter to  $\sigma(t)$  prior to using Eq. (2), namely filter A from Quinn, Tremain & Duncan (1991), with sampling 1 yr and decimation factor of 10, to suppress fast  $\simeq 80$  yr oscillations, which would otherwise disturb slower  $\simeq 280$  yr oscillations associated with resonant librations. Finally, we apply an averaging over 1 Myr running window.

The overall dynamical structure of the J3/2 resonance is determined by secular resonances  $\nu_5$ ,  $\nu_6$  at high eccentricities  $e_p \gtrsim 0.3$  and secondary resonances at lower values of  $e_p \lesssim 0.13$  (according to Morbidelli & Moons 1993, Ferraz-Mello et al. 1998, Roig & Ferraz-Mello 1999). They destabilise orbits at the borders of a stable island. The orbits inside the island exhibit very low chaotic diffusion rates, so bodies can remain there for 4 Gyr (without any non-gravitational perturbation).

Next we apply a hierarchical clustering method (Zapalá et al. 1994) to detect significant clusters. We use a standard metric in the proper element space  $(a_p, e_p, \sin I_p)$

$$\delta v = na \sqrt{\frac{5}{4} \left( \frac{\delta a_p}{a_p} \right)^2 + 2(\delta e_p^2) + 2(\delta \sin I_p)^2}. \quad (3)$$

In the following, we do not discuss the known Schubart family, which was sufficiently analysed elsewhere (Brož and Vokrouhlický 2008), but we focus on the family associated with (153) Hilda. A suitable cut-off velocity for the Hilda family seems to be  $v_{\text{cutoff}} = 150$  m/s, because the number of members does not change substantially around this value (see Figure 1). The number of members at this cut-off is 360.

The resulting plots  $(a_p, H)$ ,  $(e_p, H)$  and  $(I_p, H)$  of the Hilda family show very interesting features (see Figure 2). The distribution of semimajor axis and inclination seems

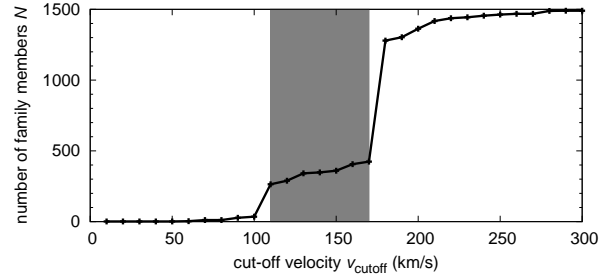


**Figure 1.** The number  $N$  of the Hilda family members versus the selected cut-off velocity  $v_{\text{cutoff}}$ .

rather even and almost independent of absolute magnitude  $H$ , but eccentricities of small asteroids (i.e., with high  $H$ ) are clearly concentrated at the outskirts of the family and depleted in the centre.

We consider these ‘ears’ in the  $(e_p, H)$  plane to be a strong indication of the ongoing Yarkovsky/YORP evolution, because they are very similar to those observed among several the Main-Belt families in the  $(a_p, H)$  plane and successfully modelled by Vokrouhlický et al. (2006b). The difference between these two cases stems from the fact, that Main-Belt families are non-resonant and the Yarkovsky/YORP effect thus perturbs semimajor axis, while in our resonant case, the same perturbation results rather in systematic changes of eccentricity. A detailed modelling of the  $e$ -distribution is postponed to Section 4.2.

Geometric albedo is a poorly known quantity. There are only six measured values for the Hilda family members: 0.064, 0.046, 0.038, 0.089, 0.044, 0.051. These were calculated from diameters included in the AstOrb catalogue, according to the relation of Bowell et al. (1989)  $\log p_V = 6.259 - 2 \log D - 0.4H$ , and compared to values in the PDS database (Davis & Neese 2002). Given the low number of values and a possibility of selection effects we prefer to assume the family members have a mean value  $p_V = 0.044$ , which corresponds to the whole J3/2 population. The size of the parent body can be then estimated to  $D_{\text{PB}} = (200 \pm 20)$  km. A test with different albedo values will be described in Section 4.4.

Size-frequency distributions  $N(>D)$  vs  $D$  of both families in the J3/2 resonance are steeper than that of background, but shallower than for usual Main-Belt families (Figure 3). This might be a common feature also in the Trojan region, e.g., the Eurybates family exhibits a similar slope with  $\gamma = (2.5 \pm 0.1)$ .

Interestingly, the part of the J3/2 population with low inclinations ( $I_p \leq 2.5^\circ$ ) has a significantly *steeper* size-frequency distribution too. Possibly, it may be a remnant of an old, totally dispersed family which is not recognisable by the HCM method today? If true, it may be a basis of a new family-identification method suitable for dispersed families. One has to subtract families identified by the HCM first and then check SFD’s in different parts of the proper-element space. Another possibility to explain this difference in SFD’s are different source populations, from which the J3/2 population was originally captured. E.g., lower-inclination bodies may originate from the Main Belt and larger-inclination from transneptunian region.

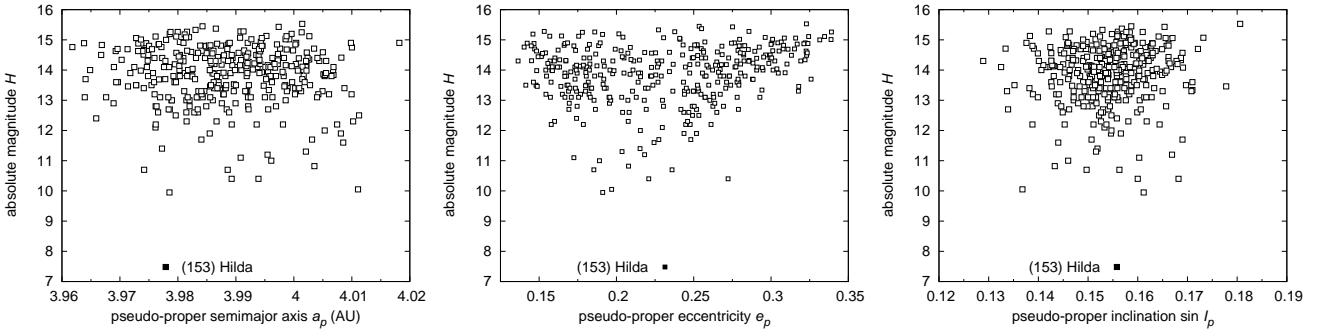


**Figure 2.** The Hilda family displayed in resonant semimajor axis  $a_p$  (left), eccentricity  $e_p$  (middle) and inclination  $\sin I_p$  (right) versus absolute magnitude  $H$ . The ‘ears’ in  $(e_p, H)$ , i.e., the concentration of small asteroids at the outskirts of the family and their depletion in the centre, are very prominent here. The family has 360 members at  $v_{\text{cutoff}} = 150$  m/s.

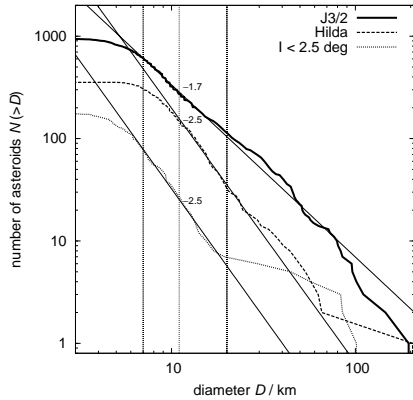


**Figure 3.** Cumulative size distributions of the J3/2 population (without families), of the Hilda family and a  $I \leq 2.5^\circ$  part of the J3/2 population. The polynomial fits of the form  $N(>D) = CD^\gamma$  are plotted as thin lines, together with the respective values of the  $\gamma$  exponent.

Finally, we have to mention the surroundings of the Hilda family. The family seems to be *separated* from the background at the  $(a_p, I_p)$  plot (Figure 4). There is a very low number of background bodies even though orbits should be stable everywhere. We confirm this statement by a direct numerical integration of test particles initially spaced evenly in the osculating element space ( $a \in (3.91, 4.01)$  AU,  $e \in (0.2, 0.3)$ ,  $I \in (4.5^\circ, 13.5^\circ)$ ). Even after 4 Gyr of evolution the particles located in the surroundings of the Hilda family remain stable. We think this indicates the Hilda family was created by a disruption of a solitary body in the J3/2 resonance.

### 3 DESCRIPTION OF THE HILDA FAMILY MODEL

To understand long-term evolution of the Hilda family, we construct a detailed model, extending efforts in Brož and Vokrouhlický (2008), which includes the following processes: (i) impact disruption, (ii) planetary migration, (iii) the Yarkovsky effect, (iv) the YORP effect, (v) collisions and spin-axis reorientations. We describe the individual parts of the model in the forthcoming subsections.

#### 3.1 Impact disruption

We use a very simple model of an isotropic disruption from the work of Farinella et al. (1994). The distribution of velocities “at infinity” follows the function

$$dN(v) = Cv(v^2 + v_{\text{esc}}^2)^{-(\alpha+1)/2}, \quad (4)$$

with the exponent  $\alpha$  being a free parameter,  $C$  a normalisation constant and  $v_{\text{esc}}$  the escape velocity from the parent body, which is determined by its size  $R_{\text{PB}}$  and mean density  $\rho_{\text{PB}}$  as  $v_{\text{esc}} = \sqrt{(8/3)\pi G \rho_{\text{PB}} R_{\text{PB}}}$ . The distribution is usually cut at a selected maximum allowed velocity  $v_{\text{max}}$  to prevent outliers. The actual initial velocities of individual bodies are generated by a straightforward Monte-Carlo code and their orientations in space are assigned randomly.

Here, we assume the velocity of fragments is independent on their size, which seems reasonable with respect to the observed even distribution of the Hilda family in the  $(a_p, H)$  and  $(I_p, H)$  planes (Figure 2). We perform also tests with non-isotropic distributions in Section 4.5.

We are also free to select initial osculating eccentricity  $e_i$  of the parent body, initial inclination  $i_i$ , as well as true anomaly  $f_{\text{imp}}$  and argument of perihelion  $\omega_{\text{imp}}$  at the time of impact disruption. All of these parameters determine the initial shape of the synthetic “Hilda” family just after the disruption of the parent body.<sup>1</sup> Initial semimajor axis  $a_i$  is not free, instead it is calculated from the initial semimajor axis of Jupiter  $a_{\text{Ji}}$  and the Kepler law, since the parent body have to be confined in the J3/2 resonance.

#### 3.2 Planetary migration

At later stages the planetary migration was most probably caused by a presence of a massive planetesimal disc. A self-consistent model for planetary migration thus would require a full N-body simulation with not only planet  $\leftrightarrow$  planetesimals interactions but also with planetesimals  $\leftrightarrow$  planetesimals interactions. This kind of model is however extraordi-

<sup>1</sup> In order to start the simulation at a required  $f_{\text{imp}}$  and  $\omega_{\text{imp}}$  we perform a short integration of the parent body together with planets using a Bulirsch–Stöer integrator (SWIFT–BS). We monitor true anomaly and argument of perihelion until secular perturbations  $\dot{f} \doteq \dot{f}_{\text{imp}}$  and  $\dot{\omega} \doteq \dot{\omega}_{\text{imp}}$ .

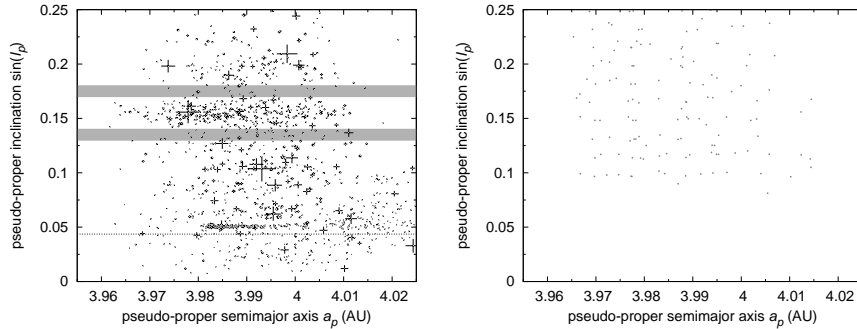


**Figure 4.** Left panel: the J3/2 region displayed at  $(a_p, I_p)$  plot. The close surroundings of the Hilda family, where only a low number of bodies is present, is highlighted by grey rectangles. The dashed line indicates the inclination  $I = 2.5^\circ$ , which was discussed with respect to the size-frequency distributions. A very prominent Schubart cluster (studied by Brož and Vokrouhlický 2008) is visible around  $\sin I_p \doteq 0.05$ . Right panel: test particles initially spaced evenly in the proper element space ( $a \in (3.91, 4.01)$  AU,  $e \in (0.2, 0.3)$ ,  $I \in (4.5^\circ, 13.5^\circ)$ ) after 4 Gyr of evolution. This test serves as a confirmation of orbital stability in the surroundings of the Hilda family.

narily CPU consuming and impractical. Usually, it is possible to drop mutual planetesimal interactions completely, which have a minor effect only, and continue with a simpler N-body model.

Another possibility is to drop even the planet  $\leftarrow$  planetesimals interactions and use a so called *analytic migration* model, with an artificial energy dissipation applied to planets. This is the only viable possibility in our case, because we need to test not only a large number of various migration scenarios but also various initial configurations of the synthetic ‘‘Hilda’’ family. Moreover, we are not interested in the evolution of the planetesimal disc and thus we need not to calculate the orbital evolution of planetesimals at all.

For this purpose we use a modified version of the symplectic SWIFT-RMVS3 integrator (Levison & Duncan 1994). We account for gravitational perturbations of the Sun and four giant planets and include the following energy dissipation term applied in every time step

$$v_x := v_x \left[ 1 + \frac{1}{v} \frac{\Delta t}{\tau_{\text{mig}}} \Delta v \exp\left(-\frac{t-t_0}{\tau_{\text{mig}}}\right) \right], \quad (5)$$

where  $v_x$  (or equivalently  $v_y, v_z$ ) denotes a velocity component of a given planet,  $v$  the absolute value of velocity,  $\Delta t$  the time step,  $\tau_{\text{mig}}$  the selected migration time scale,  $\Delta v = \sqrt{GM/a_i} - \sqrt{GM/a_f}$  the required total change of velocity (i.e., the difference of mean velocities between the initial and the final orbit),  $t$  the time and  $t_0$  some reference time.<sup>2</sup> If there are no other perturbations than (5) present, apart from the gravity of the Sun, the semimajor axis of the planet changes smoothly (exponentially) from the initial value  $a_i$  to the final  $a_f$ . We use time step  $\Delta t = 36.525$  days and the total time span of the integration is usually equal to  $3\tau_{\text{mig}}$  when planetary orbits practically stop to migrate.

It is also necessary to use an eccentricity damping formula, which simulates the effects of dynamical friction (Morbidelli et al. 2010). This enables us to model high eccentricities of planets, acquired during their resonant encoun-

ters, and their decrease to relatively low final values. The amount of eccentricity damping is characterised by a parameter  $e_{\text{damp}}$ .

A ‘softening’ parameter  $d_{\text{soft}}$  may be used to prevent close encounters between planets. It is a distance, which is artificially added to the mutual distance of planets and this way effectively weakens the gravitational perturbation.

Because inclinations of planets are not that important with respect to perturbation of minor bodies (the structure of resonances is mainly determined by planetary eccentricities), we usually start with current values of  $I$ 's.

We try to adjust initial parameters in such a way to end up at currently observed orbits, but we cannot guarantee this to happen, because we cannot account for mutual gravitational interactions and resonances in advance and we have to check final orbits at the end of integration.

Those simulations, which exhibit large discrepancy between final simulated orbits and the observed ones, are dropped. This discrepancy is measured similarly to the HCM metric (3) as a sum of  $\delta v$ 's for all planets, computed for the final simulated orbit and the currently observed one

$$\Delta v_{\text{planets}} = \sum_1^4 \delta v_i. \quad (6)$$

This way we join differences in orbital elements  $a, e, I$  into a single quantity (which has a unit of velocity). The resulting  $\Delta v_{\text{planets}} \leq 2000$  m/s is considered a good fit (refer to Figure 5).

We admit analytic migration is only a crude approximation of the real evolution, but we can use it as a first check, which kinds of migration are allowed and which are not with respect to the existence of the Hilda family. Note that very short migration time scale, like  $\tau_{\text{mig}} \simeq 3$  Myr, means almost a ‘jump’ in  $a$ . On contrary,  $\tau_{\text{mig}} \simeq 300$  Myr may correspond to a very slow, smooth late phase of migration.

Resonant elements of the J3/2 bodies are calculated online, for the actual configuration of planets. This enables us to identify dynamical processes, which perturb the synthetic ‘‘Hilda’’ family.

<sup>2</sup> It is of course possible to select different values of  $\tau_{\text{mig}}$ ,  $\Delta v$  or  $t_0$  for every planet and also to change these values in course of the simulation, in order to resemble a quite complicated migration scenarios.

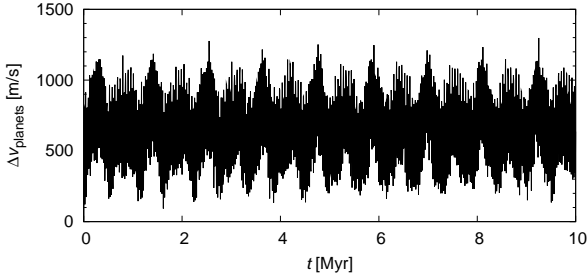


**Figure 5.** The sum  $\Delta v_{\text{planets}}$  of velocity differences between osculating orbits of planets at  $JD = 2455000.5$  and the orbits evolved over next 10 Myr. We can see the secular oscillations alone may cause a difference of  $\Delta v \leq 1500$  m/s.

### 3.3 Yarkovsky effect in a resonance

The implementation of the Yarkovsky thermal effect in the SWIFT integrator was described in detail in Brož (2006). Only minor modifications of the code were necessary to incorporate spin rate evolution, which is driven by the YORP effect (see Section 3.4).

The thermal parameter we use are reasonable estimates for C/X-type bodies:  $\rho_{\text{surf}} = \rho_{\text{bulk}} = 1300$  kg/m<sup>3</sup> for the surface and bulk densities,  $K = 0.01$  W/m/K for the surface thermal conductivity,  $C = 680$  J/kg for the heat capacity,  $A = 0.02$  for the Bond albedo and  $\epsilon_{\text{R}} = 0.95$  for the thermal emissivity parameter.

We can use exactly the same code for non-resonant and resonant bodies, because the usual drift in semimajor axis and the resonant drift in eccentricity are related “automatically” due to the gravitational part of the integrator. In Figure 6 we can see a comparison between the expected drift  $\Delta a$  in semimajor axis and the resulting drift  $\Delta e$  in eccentricity, computed for the Hilda family (see an explanation in Appendix A of Brož and Vokrouhlický 2008). The relation can be approximated as linear, where the departures from linearity are caused mainly by interactions of drifting orbits with embedded weak secular or secondary resonances.

Note that according to a standard solar model the young Sun was faint (Güdel 2007), i.e., its luminosity 4 Gyr ago was 75 % of the current  $L_{\odot}$ . We can then expect a lower insolation and consequently weaker thermal effects acting on asteroids. For the age estimates of the Hilda family it means at most 13 % larger value.

### 3.4 YORP effect

The implementation of the YORP thermal effect follows Vokrouhlický et al. (2006). We assume the following relations for the rate of angular velocity and obliquity

$$\frac{d\omega}{dt} = f(\epsilon), \quad (7)$$

$$\frac{d\epsilon}{dt} = \frac{g(\epsilon)}{\omega}, \quad (8)$$

where  $f$ - and  $g$ -functions are given by Čapek & Vokrouhlický (2004) for a set of 200 Gaussian spheres with radius  $R_0 = 1$  km, bulk density  $\rho_0 = 2500$  kg/m<sup>3</sup>, located on a circular orbit with semimajor axis  $a_0 = 2.5$  AU. The shapes of the Hilda family members are not known, so we assign artificial

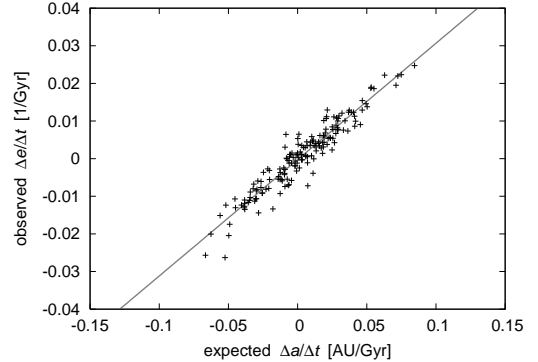


**Figure 6.** Almost linear relation between the expected drift  $\Delta a$  in semimajor axis and the simulated drift  $\Delta e$  in eccentricity, computed for 360 members of the Hilda family located inside the J3/2 resonance.

Gaussian spheres randomly to individual asteroids. We only have to scale the  $f$ - and  $g$ -functions by a factor

$$c_{\text{YORP}} \left(\frac{a}{a_0}\right)^{-2} \left(\frac{R}{R_0}\right)^{-2} \left(\frac{\rho_{\text{bulk}}}{\rho_0}\right)^{-1}, \quad (9)$$

where  $a$ ,  $R$ ,  $\rho_{\text{bulk}}$  are semimajor axis, radius and density of the simulated body,  $c_{\text{YORP}}$  is a free scaling parameter, which can account for an additional uncertainty of the YORP model. Because the values of  $f$ 's and  $g$ 's were computed for only a limited set of obliquities ( $\Delta\epsilon = 30^\circ$ ) we use interpolation by Hermite polynomials (Hill 1982) to obtain a smooth analytical function.

If the angular velocity approaches a critical value

$$\omega_{\text{crit}} = \sqrt{\frac{8}{3}\pi G \rho_{\text{bulk}}}, \quad (10)$$

we assume a mass shedding event, so we keep the orientation of the spin axis and the sense of rotation, but we reset the orbital period  $P = 2\pi/\omega$  to a random value from the interval (2.5, 9) hours. We also change the assigned Gaussian sphere to a different one, since any change of shape may result in a different YORP effect.

The differential equations (7), (8) are integrated numerically by a simple Euler integrator. The usual time step is  $\Delta t = 1000$  yr. Such a detailed model for the YORP-driven evolution of spin axes and a symplectic N-body integrator is a unique combination. An example of the results computed by the spin integrator for the Hilda family is displayed in Figure 7. The typical time scale of the spin axis evolution is  $\tau_{\text{YORP}} \simeq 500$  Myr. After  $\simeq 3$  times  $\tau_{\text{YORP}}$  most bodies have spin axes perpendicular to their orbits, what maximises the Yarkovsky drift rate of eccentricity.

### 3.5 Collisions and spin-axis reorientations

In principle, collisions may directly affect the size distribution of the synthetic “Hilda” family in course of the simulation, but we neglect this effect because most of the asteroids are large enough to remain essentially intact.

However, we include spin axis reorientations caused by collisions. We use an estimate of the time scale by Farinella et al. (1998)

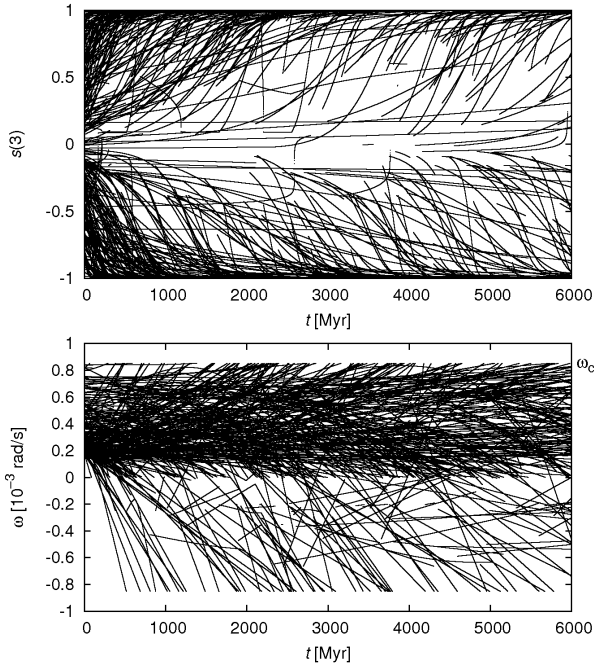


**Figure 7.** An example of the YORP-driven evolution of obliquities (namely a  $z$ -component of the spin axis unit vector, top panel) and angular velocities  $\omega$  (bottom panel) for the members of the synthetic "Hilda" family. At the beginning, all values of  $\omega$  were selected positive and spin axes were distributed isotropically. The evolution may force  $\omega$  to become negative, which simply corresponds to an opposite orientation of the spin axis. The scaling parameter was selected  $c_{\text{YORP}} = 0.33$  in this run.

$$\tau_{\text{reor}} = B \left( \frac{\omega}{\omega_0} \right)^{\beta_1} \left( \frac{D}{D_0} \right)^{\beta_2}, \quad (11)$$

where  $B = 84.5 \text{ kyr}$ ,  $\beta_1 = 5/6$ ,  $\beta_2 = 4/3$ ,  $D_0 = 2 \text{ m}$  and  $\omega_0$  corresponds to period  $P = 5 \text{ hours}$ . These values are characteristic for the Main Belt and we use them as an upper limit for the J3/2 region. Even so, the time scale is  $\tau_{\text{reor}} \simeq 3 \text{ Gyr}$  for smallest observable ( $D \simeq 5 \text{ km}$ ) bodies and reorientations are thus of minor importance only. Note the probability of the reorientation is enhanced when the YORP effect drives the angular velocity  $\omega$  close to zero.

As a summary of Section 3 we present a list of free and fixed (assumed) parameters of our model in Tables 1 and 2. The problem is we cannot tune all 24 parameters together, since the 24-dimensional space is enormous. We thus first select a reasonable set of impact parameters 15.–24., keep them fixed, and experiment with migration parameters 1.–14. We test roughly  $10^3$  migration scenarios. Then, in the second step, we vary impact parameters, for a single (successful) migration scenario, and check the sensitivity of results.

## 4 RESULTS

We discuss our results on the evolution of the synthetic "Hilda" family separately: (i) for the planetary migration, (ii) for the Yarkovsky/YORP evolution. Later on in Section 4.3 we match both results together.

**Table 1.** Free parameters of our Hilda family model.

no.	parameter	description
1.	$a_{\text{Ji}}$	initial semimajor axis of Jupiter
2.	$a_{\text{Si}}$	Saturn
3.	$a_{\text{Ui}}$	Uranus
4.	$a_{\text{Ni}}$	Neptune
5.	$e_{\text{Ji}}$	initial eccentricity of Jupiter
6.	$e_{\text{Si}}$	Saturn
7.	$e_{\text{Ui}}$	Uranus
8.	$e_{\text{Ni}}$	Neptune
9.	$\tau_{\text{mig}}$	migration time scale
10.	$e_{\text{dampJ}}$	eccentricity damping for Jupiter
11.	$e_{\text{dampS}}$	Saturn
12.	$e_{\text{dampU}}$	Uranus
13.	$e_{\text{dampN}}$	Neptune
14.	$d_{\text{soft}}$	'softening' parameter
15.	$e_i$	initial eccentricity of the parent body
16.	$i_i$	initial inclination
17.	$f_{\text{imp}}$	true anomaly at the impact disruption
18.	$\omega_{\text{imp}}$	argument of perihelion
19.	$\alpha$	slope of the velocity distribution
20.	$v_{\text{max}}$	maximum velocity of fragments
21.	$R_{\text{PB}}$	radius of parent body
22.	$\rho_{\text{PB}}$	bulk density
23.	$p_V$	geometric albedo of fragments
24.	$c_{\text{YORP}}$	efficiency of the YORP effect

**Table 2.** Fixed (assumed) parameters of the Hilda family model. There is also a number of less important parameters, like the thermal ones ( $\rho_{\text{surf}}$ ,  $K$ ,  $C$ ,  $A$ ,  $\epsilon_{\text{IR}}$ ) or collisional ( $B$ ).

no.	parameter	description
25.	$a_{\text{Jf}}$	final semimajor axis of Jupiter
26.	$a_{\text{Sf}}$	Saturn
27.	$a_{\text{Uf}}$	Uranus
28.	$a_{\text{Nf}}$	Neptune
29.	$a_i$	initial semimajor axis of the parent body
30.	$N(<H)$	(observed) absolute magnitude distribution

### 4.1 Results on planetary migration

In the first test we compute an evolution of the synthetic "Hilda" family during planetary migration phase for the following parameter space (these are not intervals but lists of values):  $a_{\text{Ji}} = (5.2806 \text{ and } 5.2027) \text{ AU}$ ,  $a_{\text{Si}} = (8.6250, 8.8250, 9.3000) \text{ AU}$ ,  $a_{\text{Ui}} = (18.4479, 12.3170) \text{ AU}$ ,  $a_{\text{Ni}} = (28.0691, 17.9882) \text{ AU}$ ,  $e_{\text{Ji}} = (0.065, 0.045)$ ,  $e_{\text{Si}} = (0.08, 0.05)$ ,  $e_{\text{Ui}} = (0.06, 0.04)$ ,  $e_{\text{Ni}} = (0.02, 0.01)$ ,  $\tau_{\text{mig}} = (0.3, 3, 30, 300) \text{ Myr}$ ,  $e_{\text{dampJ}} = 1 \cdot 10^{-11}$ ,  $e_{\text{dampS}} = 1 \cdot 10^{-11}$ ,  $e_{\text{dampU}} = 0$ ,  $e_{\text{dampN}} = 2 \cdot 10^{-11}$ ,  $d_{\text{soft}} = 0.0 \text{ AU}$ . Impact parameters were fixed except  $f_{\text{imp}}$ :  $e_i = 0.13851525$ ,  $i_i = 7.825811^\circ$ ,  $f_{\text{imp}} = (0^\circ, 180^\circ)$ ,  $\omega_{\text{imp}} = 30^\circ$ ,  $\alpha = 3.25$ ,  $v_{\text{max}} = 300 \text{ m/s}$ ,  $R_{\text{PB}} = 93.5 \text{ km}$ ,  $\rho_{\text{PB}} = 1300 \text{ kg/m}^3$ .

The synthetic "Hilda" family has 360 bodies in case of short simulations ( $\tau_{\text{mig}} = 0.3$  or  $3 \text{ Myr}$ ). In case of longer simulations we create 60 bodies only (not 360 as the observed Hilda family). Their absolute magnitudes (sizes) were selected randomly from 360 observed values. It is a minimum number of bodies necessary to compare the distributions of eccentricities. We performed tests with larger numbers and the differences do not seem significant. Even though the pa-

parameter space is rather limited, the number of simulations is 3072 and given the integration time span required ( $3\tau_{\text{mig}}$ ) it is a computationally demanding task.

A comparison with current planetary orbits shows we have to exclude approximately one half of migration scenarios which do not correspond to the current Solar System. One of the reasons for unsuccessful scenarios is that a compact configuration of planets is inherently unstable. If the migration time scale is too large or the eccentricity damping too low, it may result in a violent instability, close encounters between planets and eventually an unrealistic final configuration.

Major perturbations acting on the synthetic "Hilda" family can be seen in Figure 8. The family usually experiences a steady drift in semimajor axis, because it is coupled to Jupiter, and several 'kicks' in pseudo-proper eccentricity. Inclinations of bodies are not perturbed.

We identified the perturbations as secondary resonances between the libration frequency  $f_{J3/2}$  of an asteroid captured in the J3/2 resonance and the frequency  $f_{1J-2S}$  of the critical argument of Jupiter–Saturn 1:2 resonance (see Kortenkamp et al. 2004 or Morbidelli et al. 2005 for case of Trojans)

$$nf_{J3/2} = f_{1J-2S}, \quad (12)$$

where  $n$  is a small integer number,  $n = 2, 3$  or  $4$  in our case.<sup>3</sup> We can see the evolution of resonant semimajor axes and the corresponding dominant frequencies, computed by means of periodogram, in Figure 9.

Because the resonances are localised — they act only at particular values of semimajor axes of planets — it is *not* necessary to have a dense grid in  $a_{Ji}$ ,  $a_{Si}$  parameters. Essentially, there are only three situations, when the Hilda family is strongly perturbed, otherwise the spread in  $e$  does not change much in course of time.

A very simple test, which allows us to quickly select allowed migration scenarios, is the number of remaining "Hilda" family members. We may assume the depletion by dynamical effect was probably low (say 50% at most), otherwise we would obtain much larger large parent body than  $D \simeq 200$  km, which has much lower probability of a collisional disruption. Numbers of remaining bodies  $N_{\text{left}}$  versus initial conditions for planets is displayed in Figure 10.

Low number of remaining bodies  $N_{\text{left}}$  means either the family had to be formed later (when the resonant perturbations are low) or this migration scenario is not allowed. The same applies to the dispersion of  $e$ -distribution: if it is too large compared to the observed Hilda family, the synthetic "Hilda" had to be formed earlier or the scenario is not allowed. Our results indicate that:

- (i) a faster migration time scale  $\tau_{\text{mig}} \simeq 0.3$  Myr to 30 Myr is preferred over slower time scales;
- (ii) Jupiter and Saturn were not in the most compact configuration ( $a_{Ji} = 5.2806$  AU,  $a_{Si} = 8.6250$  AU) at the time when the "Hilda" family was created;
- (iii) initial configuration of Uranus and Neptune is not

<sup>3</sup> We also looked for secondary resonances connected with 3:7, 4:9 and 2:5 Jupiter–Saturn resonances, but there are no significant perturbations visible.

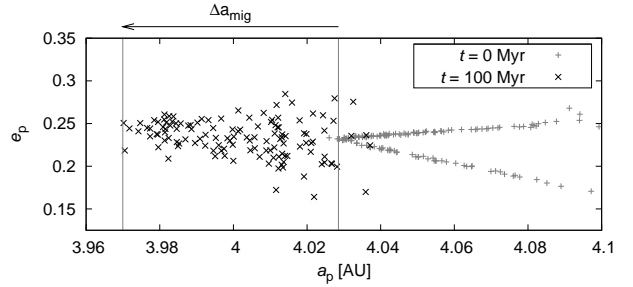


**Figure 8.** A usual evolution of the synthetic "Hilda" family in the pseudo-proper semimajor axis vs eccentricity plot. The initial ( $t = 0$  Myr) and final stages ( $t = 100$  Myr) are plotted. The migration time scale was  $\tau_{\text{mig}} = 30$  Myr in this particular example. The arrow indicates a total change of the position of the J3/2 resonance due to migration of Jupiter.

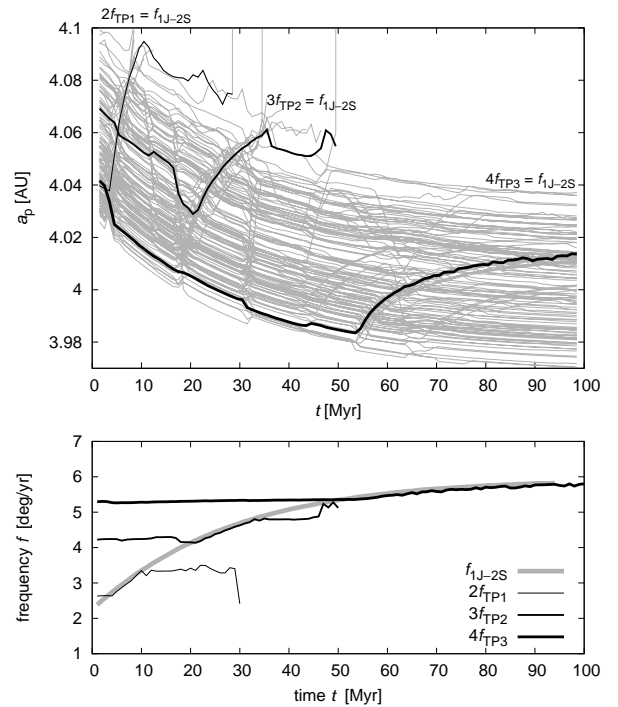


**Figure 9.** Top panel: pseudo-proper semimajor axis  $a_p$  vs time  $t$  for synthetic "Hilda" family, evolving under the influence of migrating planets with the time scale  $\tau_{\text{mig}} = 30$  Myr. Bottom panel: computed dominant frequencies  $f_{J3/2}$  of librations in the J3/2 resonance vs time, for three selected test particles. We do not plot the frequency itself but a selected multiple of it  $nf_{J3/2}$ . The frequency of Jupiter–Saturn 1:2 mean motion critical argument is also calculated. Captures in the secondary resonances of type  $nf_{J3/2} = f_{1J-2S}$  are clearly visible.

very important, as these planets do not produce direct perturbations on asteroids located in the J3/2 resonance.

We failed to reproduce scenarios when Uranus and Neptune are in a compact configuration and migrate slowly ( $\tau_{\text{mig}} = 30$  or 300 Myr). Nevertheless, there are few successful runs, where Uranus and Neptune encounter each other and end up close to their current orbits.

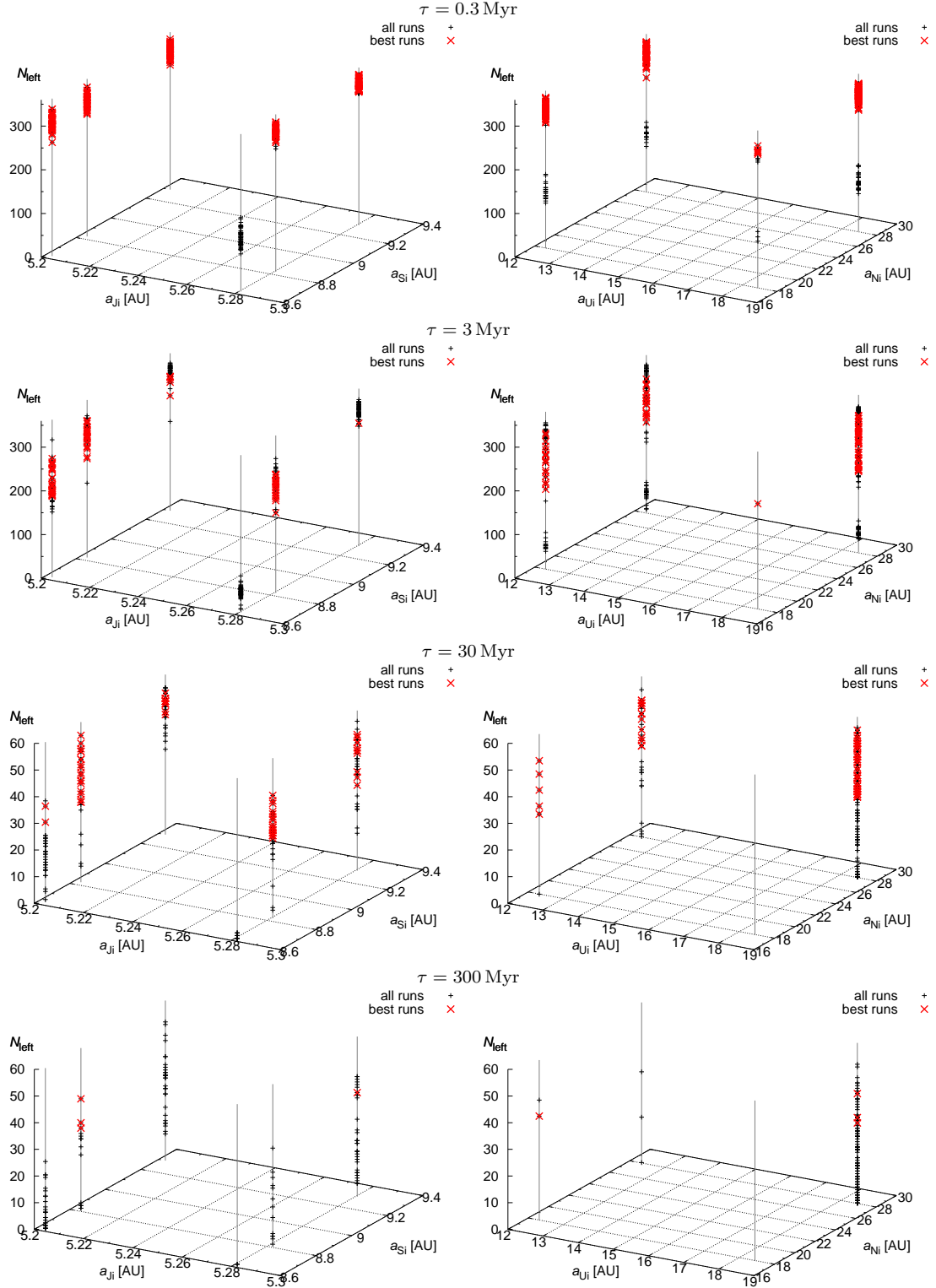


**Figure 10.** Number of remaining bodies  $N_{\text{left}}$  from synthetic “Hilda” family versus initial conditions for planets ( $a_{Ji}$ ,  $a_{Si}$ ,  $a_{Ui}$ ,  $a_{Ni}$ ) and time scale of migration  $\tau_{\text{mig}}$ . The ranges of remaining free parameters are mentioned in the text. We only plot successful migration scenarios with  $\Delta v_{\text{planets}} \leq 2000$ . The best runs, for which we also obtain a reasonable fit of the observed Hilda family, are indicated by red crosses. They are defined by conditions  $N_{\text{left}} \geq 180$  or 30 (i.e., 50% of the initial number of bodies) and median Kolmogorov–Smirnov distance  $D_{KS} \leq 0.2$  (these are determined after the subsequent Yarkovsky/YORP evolution, see Section 4.3).

## 4.2 Results on Yarkovsky/YORP evolution

We start a simulation with an impact disruption of the parent body, described by parameters 15.–23., and create 360 fragments. Subsequent evolution of the synthetic "Hilda" family due to the Yarkovsky/YORP effect is computed for up to 6 Gyr. Planets remain on their current orbits all the time, there is no migration in this test. A typical outcome of the simulation is displayed in Figure 11.

Due to the extremely long integration time span and large number of bodies we were able to compute only four simulations with the following values of true anomaly and YORP efficiency:

- (i)  $f_{\text{imp}} = 0^\circ$ ,  $c_{\text{YORP}} = 0$ ;
- (ii)  $f_{\text{imp}} = 180^\circ$ ,  $c_{\text{YORP}} = 0$ ;
- (iii)  $f_{\text{imp}} = 0^\circ$ ,  $c_{\text{YORP}} = 1$ ;
- (iv)  $f_{\text{imp}} = 0^\circ$ ,  $c_{\text{YORP}} = 0.33$ .

The remaining parameters were fixed:  $e_i = 0.13851525$ ,  $i_i = 7.825811^\circ$ ,  $\omega_{\text{imp}} = 30^\circ$ ,  $\alpha = 3.25$ ,  $v_{\text{max}} = 300$  m/s,  $R_{\text{PB}} = 93.5$  km,  $\rho_{\text{PB}} = 1300$  kg/m<sup>3</sup>,  $p_V = 0.044$ .

We are mainly concerned with the distribution of eccentricities  $e_p$ , because the observed family has an extremely large spread of  $e_p$ 's, while the synthetic family is very compact. For this purpose we constructed a Kolmogorov–Smirnov test (Press et al. 1999) of the cumulative distributions  $N(>e)$

$$D_{\text{KS}} = \max_{0 < e < 1} |N(>e)_{\text{syn}} - N(>e)_{\text{obs}}|, \quad (13)$$

which provides a measure of difference between the synthetic "Hilda" family, at a given time, and the observed Hilda family (see Figure 12 for an example). The results of the KS tests are summarised in Figure 13 (first four panels).

We also construct a modification of the KS test, which aligns the *medians* of the  $N(>e)$  distributions prior to the calculation of the KS statistics. Our motivation is that it is possible to start the simulation with a lower or higher value of the initial eccentricity  $e_i$  and this way shift the whole synthetic family. We verified this statement by numerical tests. By doing this 'trick' we overcome the need to run simulations with different  $e_i$ 's.

The results of 'median KS' tests are presented in Figure 14. Moreover, we use a slightly different definition of the observed Hilda family to test the robustness of the results ( $v_{\text{cutoff}} = 150$  m/s is the same, but the family is selected from an older version of the catalogue, so it contains 233 bodies only). Nevertheless, the tests stay compatible with the previous version.<sup>4</sup>

There is an easy possibility to assess the sensitivity of results with respect to the  $v_{\text{max}}$  parameter too, without the need to compute the simulation again. We simply select bodies fulfilling the condition  $v < v'_{\text{max}}$ , with  $v'_{\text{max}} = 200, 100$  or  $50$  m/s, and recompute only the KS statistics for this subset. The results are plotted in Figures 13 and 14 as thin lines. We can state values lower than  $v_{\text{max}} \simeq 100$  m/s are surely excluded.

<sup>4</sup> The differences at late times stem from the fact that the evolved synthetic family is sometimes depleted of bodies at its border and due to the shift of medians it may become more compatible with the observed Hilda family.

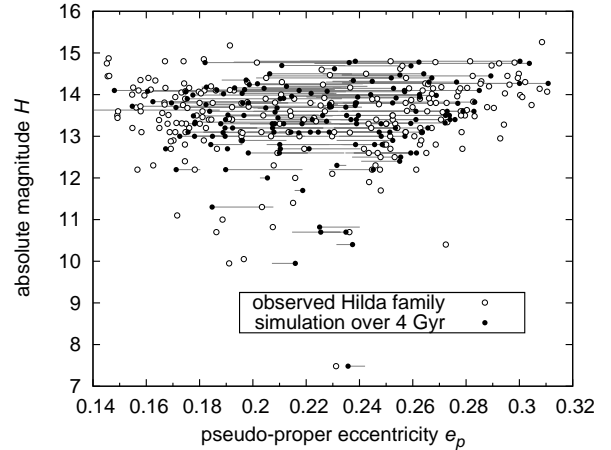


**Figure 11.** Eccentricity vs absolute magnitude plot for the synthetic "Hilda" family after 4 Gyr of evolution and its comparison with the observed Hilda family. Lines indicate a total change of eccentricities over 4 Gyr.

As a preliminary conclusion we may say that all simulations point to a large age of the Hilda family. The  $e$ -distributions are most compatible with the observed family for ages  $t = (4.0 \pm 1.0)$  Gyr, which suggests the Hilda family indeed experienced the planetary migration period. The large uncertainty stems from the fact that the runs including the YORP effect ( $c_{\text{YORP}} \geq 0.33$ ) tend to produce ages at a lower limit of the interval while the YORP-less runs (with  $c_{\text{YORP}} = 0$ ) tend to the upper limit.

We have to admit it is possible to obtain a good fit of the observed  $e$ -distribution even without planetary migration if we include the YORP effect with  $c_{\text{YORP}} = 0.33$  (see Figure 12). Nevertheless, the age corresponding to the best fit ( $t \simeq 3.8$  to  $4.0$  Gyr) leads us to a conclusion the Hilda family was likely created during late phases of planetary migration which are dated by the Late Heavy Bombardment to  $t_{\text{LHB}} \simeq 3.85$  Gyr (Gomes et al. 2005).

## 4.3 Matching results together

Even though we do not perform a joint integration which includes both the planetary migration and Yarkovsky/YORP effect, we try to match the previous results from Sections 4.1 and 4.2 together. We do it using a straightforward Monte–Carlo approach: (i) we take the pseudo-proper eccentricities  $e_{\text{mig}}$  of bodies at the end of planetary migration from Section 4.1; (ii) we compute total Yarkovsky/YORP drifts  $\Delta e_{\text{YE}}$  in eccentricity from Section 4.2; (iii) we assign every body a drift randomly ( $e_{\text{final}} = e_{\text{mig}} + \Delta e_{\text{YE}}$ ) and this way we construct an evolved synthetic family.<sup>5</sup> Finally, we compare the synthetic family to the observed Hilda family by computing a Kolmogorov–Smirnov test for  $N(>e_{\text{final}})$  and  $N(>e)_{\text{obs}}$  distributions.

To avoid problems with low number of bodies (60 in case

<sup>5</sup> Note gravitational perturbation, caused by planetary migration, is independent of size (mass), so a large body may be easily found at the outskirts of the family. This is another reason for the random assignment of Yarkovsky/YORP drifts.

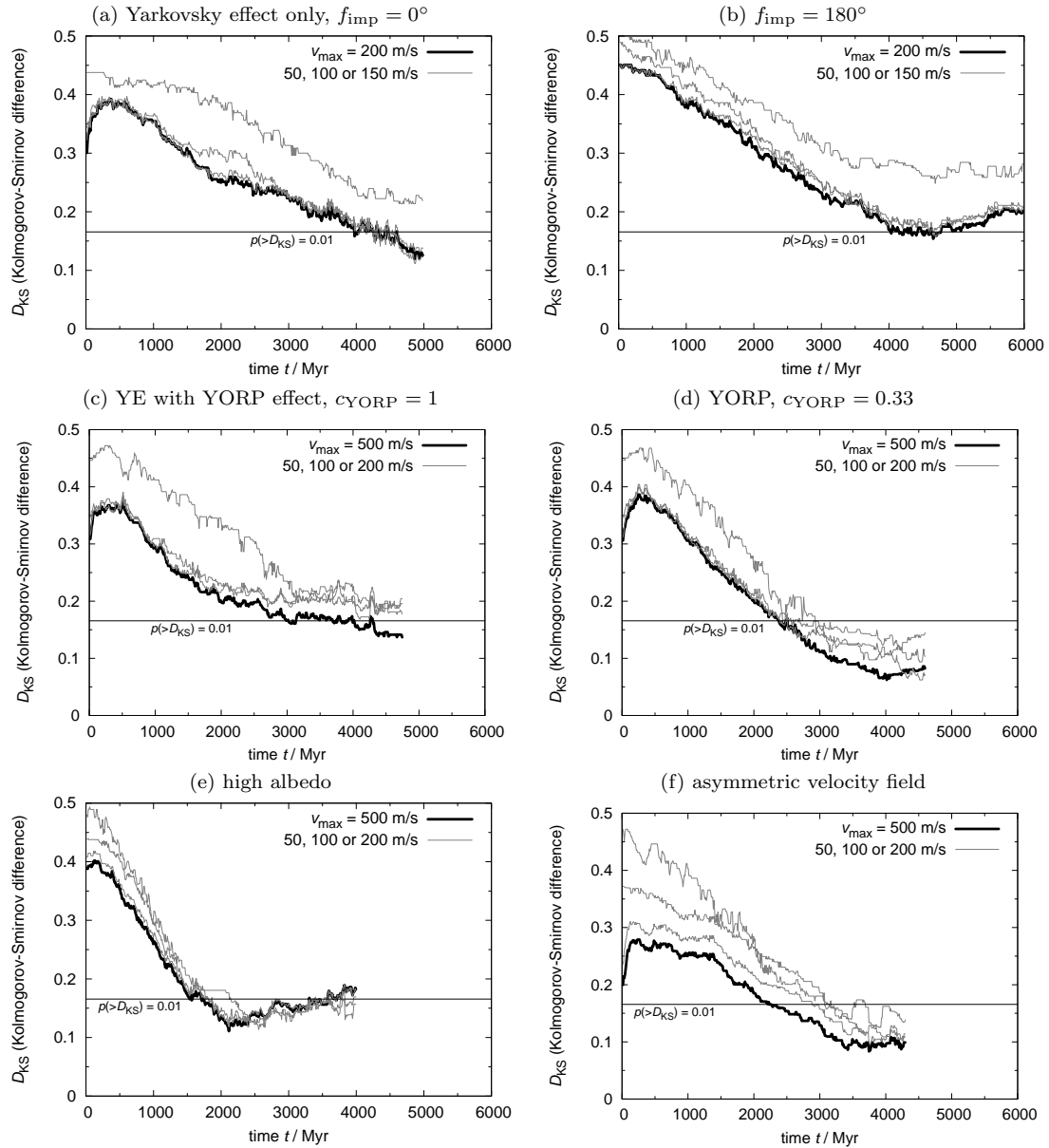


**Figure 13.** Kolmogorov-Smirnov tests of the synthetic “Hilda” family: (a) no migration, only initial disruption (at anomaly  $f_{\text{imp}} = 0^\circ$ ,  $\varpi_{\text{imp}} = 30^\circ$ ) and subsequent Yarkovsky evolution; (b) the case with  $f_{\text{imp}} = 180^\circ$ ; (c) including the YORP effect; (d) YORP with efficiency factor  $c_{\text{YORP}} = 0.33$ ; (e) high albedo values (i.e., small bodies); (f) strongly asymmetric velocity field.

of planetary migration), we perform the above assignment 100 times, always with a different random seed. We then take a median of the 100 KS statistics as a result for one particular run. We do not plot the median  $D_{\text{KS}}$  vs initial conditions separately, we instead refer back to Figure 10, where red crosses indicate successful runs with  $D_{\text{KS}} \leq 0.2$ .

We confirm the conclusions from Section 4.1 — those migration scenarios which preserve most of number of family members (i.e., high  $N_{\text{left}}$ ) are the same, for which we can find a good fit of eccentricity distribution (low  $D_{\text{KS}}$ ).

Another important test was devoted to the impact parameters, which were varied in a relatively large steps:  $e_i = (0.11851525, 0.14851525, \dots)$ ,  $i_i = (6.825811^\circ, 8.825811^\circ)$ ,  $f_{\text{imp}} = (45^\circ, 90^\circ, 135^\circ)$ ,  $\omega_{\text{imp}} = (60^\circ, 90^\circ)$ ,  $\alpha = (2.25, 4.25)$ ,  $v_{\text{max}} = (200, 400) \text{ m/s}$ ,  $R_{\text{PB}} = (83.5, 103.5) \text{ km}$ ,  $\rho_{\text{PB}} =$

$(1000, 2000) \text{ kg/m}^3$ . The migration parameters were fixed this time (they correspond to one successful migration scenario):  $a_{\text{Ji}} = 5.2806 \text{ AU}$ ,  $a_{\text{Si}} = 8.8250 \text{ AU}$ ,  $a_{\text{Ui}} = 18.4479 \text{ AU}$ ,  $a_{\text{Ni}} = 28.0691 \text{ AU}$ ,  $e_{\text{Ji}} = 0.065$ ,  $e_{\text{Si}} = 0.08$ ,  $e_{\text{Ui}} = 0.06$ ,  $e_{\text{Ni}} = 0.02$ ,  $\tau_{\text{mig}} = 3 \text{ Myr}$ ,  $e_{\text{dampJ}} = 1 \cdot 10^{-11}$ ,  $e_{\text{dampS}} = 1 \cdot 10^{-11}$ ,  $e_{\text{dampU}} = 0$ ,  $e_{\text{dampN}} = 2 \cdot 10^{-11}$ ,  $d_{\text{soft}} = 0.0 \text{ AU}$ .

The resulting Kolmogorov–Smirnov distances  $D_{\text{KS}}$  are displayed in Figure 15. We see no strong preference for any of the impact parameters, though we may improve or worsen a given fit by changing them ( $D_{\text{KS}}$  differs by 0.1 at most). Note that the selection of impact parameters is rather extreme, we do not expect they may ever be out of these bounds. Hence, our conclusion is the impact parameters are less important than the parameters related to migration.

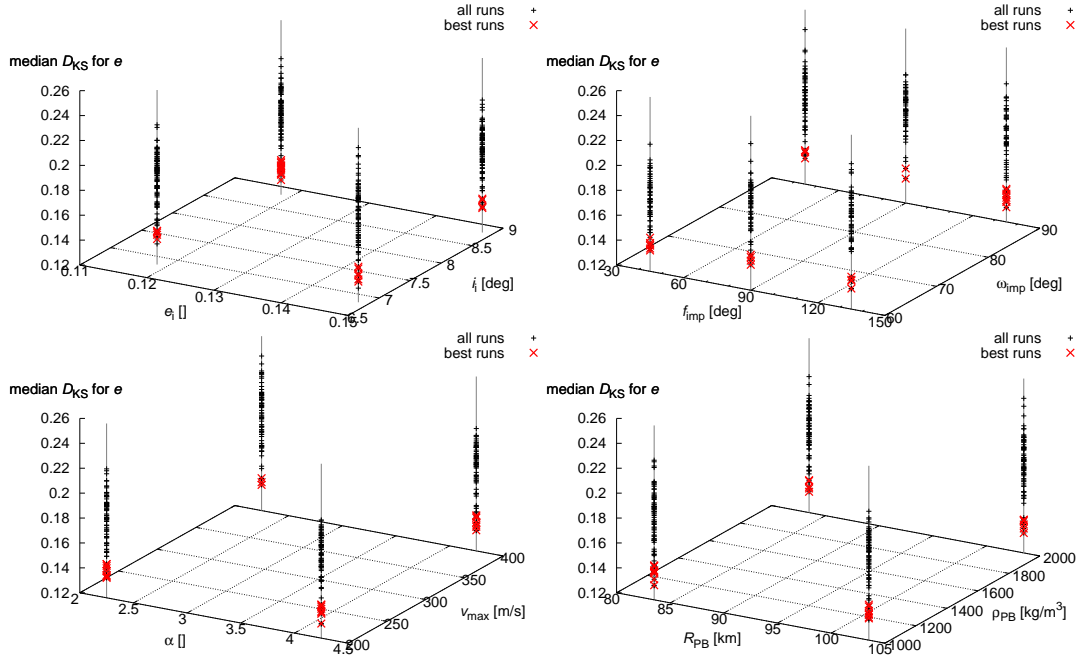


**Figure 15.** Kolmogorov–Smirnov statistics  $D_{KS}$  for various initial conditions of an impact disruption: initial eccentricity  $e_i$ , inclination  $i_i$ , true anomaly  $f_{imp}$ , argument of perihelion  $\omega_{imp}$ , exponent  $\alpha$ , maximum velocity  $v_{max}$ , radius of the parent body  $R_{PB}$  and its bulk density  $\rho_{PB}$ . The values of remaining parameters related to migration are mentioned in the text. The best runs are indicated by red crosses.

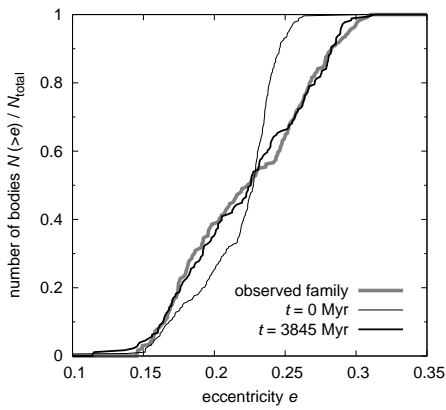


**Figure 12.** A cumulative distribution  $N(>e)$  of eccentricities for (i) the observed Hilda family, (ii) the synthetic “Hilda” family at time  $t = 0$  (just after the impact disruption), (iii) evolved due to the Yarkovsky/YORP effect (at time  $t = 3845$  Myr). In this figure we show the best fit for the simulation with parameters  $f_{imp} = 0^\circ$ ,  $c_{YORP} = 0.33$ . Note the ‘bended’ shape of the observed distribution corresponds to the ‘ears’ on the  $(e_p, H)$  plot (Figure 2). There is no perturbation by planetary migration in this particular case.

#### 4.4 Alternative hypothesis: high albedos of small asteroids

We have to admit there might be another explanations for the observed large eccentricity dispersion of the Hilda family. We thus discuss two alternative scenarios without planetary migration: (i) high albedos of small asteroids (i.e., larger Yarkovsky/YORP drift); (ii) strongly asymmetric velocity field after impact (like that of the Veritas family).

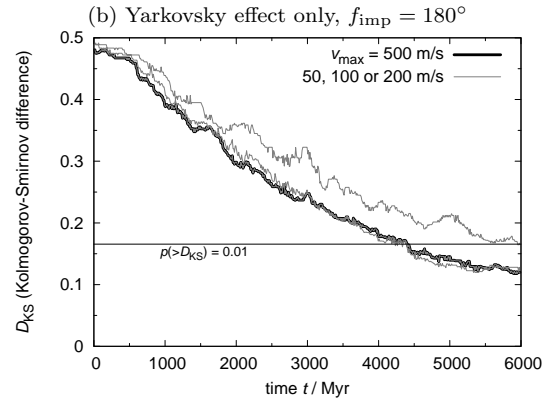


**Figure 14.** A different Kolmogorov-Smirnov test of the Hilda family with aligned medians of  $e$ : the case with Yarkovsky effect and  $f_{imp} = 180^\circ$  for direct comparison with panel (b) in Figure 13.

Albedo is the most important unknown parameter, which can affect results on the Yarkovsky/YORP evolution. Fernández et al. (2009) measured albedos of small Trojan asteroids and found a systematically larger values that for large Trojans. If we assume the J3/2 asteroids behave similarly to Trojans, we may try a simulation with a rather high value of geometric albedo  $p_V = 0.089$  (compared to previous  $p_V = 0.044$ ). Moreover, we decrease density  $\rho_{bulk} = 1200 \text{ kg/m}^3$ , increase maximum velocity of fragments  $v_{max} = 500 \text{ m/s}$  and select true anomaly  $f_{imp} = 90^\circ$  to maximise the spread of  $e_p$ ’s.

The KS test is included in Figure 13, panel (e). The most probable age seems to be  $(2.3 \pm 0.5) \text{ Gyr}$  only in this case. Let us conclude that a high albedo explanation is the

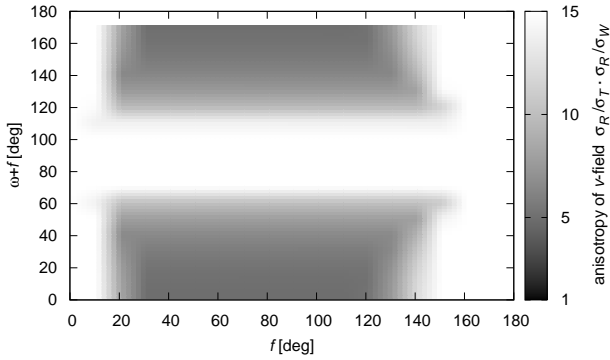


**Figure 16.** Anisotropy of the velocity field in the Veritas family and its dependence on the geometry (true anomaly  $f$  and argument of pericentre  $\omega$ ). The anisotropy parameter, i.e., the ratio of velocity dispersions in  $R$ ,  $T$  and  $W$  directions:  $\max(\sigma_R/\sigma_T, \sigma_T/\sigma_R) \cdot \max(\sigma_R/\sigma_W, \sigma_W/\sigma_R)$  is never smaller than 4. We use Gauss equations to compute velocity components  $v_R$ ,  $v_T$ ,  $v_W$  from orbital elements  $a$ ,  $e$ ,  $I$ . The effect of chaotic diffusion acting on eccentricity  $e$  in resonances was compensated by shifting the respective asteroids in eccentricity ‘backwards’.

oretically possible, but not very probable, because any collisional family should likely have the same albedo for large and small members, since they originate from the same parent body.

#### 4.5 Alternative hypothesis: strongly asymmetric velocity field

Another possibility is that the original velocity was highly anisotropic. A well known example from the Main Belt is the Veritas family. Let us assume the anisotropy is of the order of Veritas, i.e., approximately 4 times larger in one direction (see Figure 16). Note that the Veritas is a young family and can be modelled precisely enough to compensate for chaotic diffusion in resonances (Nesvorný et al. 2003, Tsiganis et al. 2007). This family is characteristic by a large spread in inclinations, which corresponds to large  $W$ -components of velocities. In case of the Hilda family we multiply by 4 the  $R$ -components of initial velocities to maximise the dispersion of eccentricities at most favourable geometry of disruption ( $f_{\text{imp}} \doteq 0$ ).

The fit in Figure 13, panel (f) is seemingly better at the beginning of the simulation, but bodies on unstable orbits are quickly eliminated and the fit gets much worse at  $t \simeq 500$  Myr. We can see the synthetic ‘Hilda’ family is similar to the observed Hilda family quite early (at  $t \simeq 2.5$  Gyr), however the best fit is at later times ( $t \simeq 3.5$  Gyr), so there is no significant benefit compared to isotropic cases.

The conclusion is asymmetric velocity field is not a likely explanation of the  $e_p$  dispersion. Note that majority of Main-Belt families can be also modelled assuming isotropic initial velocity fields.

### 5 COLLISIONAL PROBABILITIES AMONG THE J3/2 POPULATION

Let us estimate a collisional activity in the J3/2 region by means of a simple stationary model, namely the likeli-

hood of a Hilda-family-forming event. In our case, the target (parent body) diameter  $D_{\text{target}} = 200$  km, mean impact velocity  $V_{\text{imp}} = 4.78$  km/s (Dahlgren 1998), strength  $Q_D^* = 4 \cdot 10^5$  J/kg (it scales as  $D^2$  in gravity regime) and thus the necessary impactor size (Bottke et al. 2005)

$$d_{\text{disrupt}} = (2Q_D^*/V_{\text{imp}}^2)^{1/3} D_{\text{target}} \simeq 65 \text{ km}. \quad (14)$$

Number of  $\geq 65$  km projectiles is dominated by Main-Belt bodies:  $n_{\text{project}} = 160$ , according to (Bottke et al. 2006), and we have only one 200 km target in the J3/2 region, so  $n_{\text{target}} = 1$ . An intrinsic collisional probability for Hilda vs Main Belt collisions  $P_i = 6.2 \times 10^{-19} \text{ km}^{-2} \text{ yr}^{-1}$  (Dahlgren 1998) and corresponding frequency of disruptions is

$$f_{\text{disrupt}} = P_i \frac{D_{\text{target}}^2}{4} n_{\text{project}} n_{\text{target}} \simeq 10^{-12} \text{ yr}^{-1}. \quad (15)$$

Over the age of the Solar System  $T_{\text{SS}} \simeq 4$  Gyr (after LHB), we have a very low number of such events  $n_{\text{events}} = T_{\text{SS}} f_{\text{disrupt}} \simeq 0.004$ .

Our preliminary conclusion, based on current collisional rates, is thus it is very unlikely to have a large number of Hilda-size families in the J3/2 region. Even the existence of a single family with a 200 km parent body seems improbable, but given the fact Hilda family is dynamically very old ( $\leq 4$  Gyr), it may indicate that collisional activity was substantially higher in the past, e.g., during the Late Heavy Bombardment.

We can think of two projectile populations: (i) transient decaying planetesimal disk; (ii) D-type asteroids captured in the J3/2. Models like that of Levison et al. (2009) suggest the decay time scale of the planetesimal disk is of the order 10 to 100 Myr and the flux of impactors might have been 100 times larger than today. Higher mean collisional velocities, due to projectiles on high- $e$  and high- $i$  orbits, are also favourable. If we assume these reasonable numbers:  $V_{\text{imp}} = 20$  km/s,  $d_{\text{disrupt}} = 25$  km,  $n_{\text{project}} = 160000$  and the time span of the LHB  $T_{\text{LHB}} = 200$  Myr, we end up with the number of events  $n_{\text{events}} = 0.2$ , which is closer to one.

Regarding the captured D-type asteroids, they were probably not so numerous ( $n_{\text{project}}$  was lower), but they might have had larger  $P_i$  and substantially longer  $T_{\text{LHB}}$ . Again, the number of event may be closer to one.

## 6 CONCLUSIONS

The Hilda family proved to be one of the oldest families in the Main Asteroid Belt. Since it is embedded inside the 3/2 mean-motion resonance with Jupiter, its orbital evolution is coupled to this giant planet. In case the Hilda family was created during planetary migration, which seems to us likely, the major perturbations of the family were due to secondary resonances between librations and the Jupiter–Saturn 1:2 critical argument. A gentle ‘kick’ of eccentricities is necessary and then a subsequent evolution due to the Yarkovsky/YORP effect to bring the family to the currently observed state.

Note there are two competing effects: during a period of fast migration the probability of a collisional disruption of parent body is significantly enhanced, but on the other hand, strong perturbations present in a compact planetary configuration usually destroy the synthetic ‘Hilda’ family.

Emerging signs, that orbital evolution of planets was rather violent and close encounters between planets were probably present (Nesvorný et al. 2007, Brassier et al. 2010), might be consistent with our model of the Hilda family, since we see a preference of fast migration time scales. We postpone a study of more complicated migration scenarios, like that of ‘jumping Jupiter’ (Morbidelli et al. 2010), to future work.

Regarding future improvements of our model, knowledge of geometric albedos for a large number of small asteroids may significantly help and decrease uncertainties. The WISE infrared mission seems to be capable to obtain this data in near future.

## ACKNOWLEDGEMENTS

We thank H. Levison for his code on eccentricity damping and D. Čapek for sending us the YORP effect data in an electronic form.

The work of MB and DV has been supported by the Grant Agency of the Czech Republic (grants 205/08/0064 and 205/08/P196) and the Research Program MSM0021620860 of the Czech Ministry of Education. We also acknowledge the usage of computers of the Observatory and Planetarium in Hradec Králové.

## REFERENCES

- Bottke W.F., Durda D.D., Nesvorný D., Jedicke R., Morbidelli A., Vokrouhlický D., Levison H.F., 2005, *Icarus*, 175, 111
- Bottke W.F., Nesvorný D., Grimm R.E., Morbidelli A., O’Brien D.P., 2006, *Nature*, 439, 821
- Bottke W.F., Vokrouhlický D., Brož M., Nesvorný D., Morbidelli A., 2001, *Science*, 294, 1693
- Bowell E., Hapke B., Domingue D., Lumme K., Peltoniemi J., Harris A.W., 1989, in Binzel R.P., Gehlers T., Matthews M.S., eds., *The University of Arizona Press*, Tucson, p. 549
- Brassier R., Morbidelli A., Gomes R., Tsiganis K., Levison H.F., 2010, *A&A*, 507, 1053
- Brož M., 2006, PhD thesis, Charles Univ.
- Brož M., Vokrouhlický D., 2008, *MNRAS*, 390, 715
- Čapek D., Vokrouhlický D., 2004, *Icarus*, 172, 526
- Dahlgren M., 1998, *A&A*, 336, 1056
- Davis D.R., Neese C., eds., 2002, *Asteroid Albedos*. EAR-A-5-DDR-ALBEDOS-V1.1. NASA Planetary Data System
- Farinella P., Froeschlé C., Gonczi R., 1994, in Milani A., Di Martino M., Cellino A., eds., *Asteroids, comets, meteors 1993*. Kluwer Academic Publishers, Dordrecht, p. 205
- Farinella P., Vokrouhlický D., Hartmann W.K., 1998, *Icarus*, 132, 378
- Fernández Y.R., Jewitt D., Ziffer J.E., 2009, *AJ*, 138, 240
- Ferraz-Mello S., Michtchenko T.A., Nesvorný D., Roig F., Simula A., 1998, *P&SS*, 46, 1425
- Gomes R., Levison H.F., Tsiganis K., Morbidelli A., 2005, *Nature*, 435, 466
- Güdel M., 2007, *Living Rev. Solar Phys.*, 4, 3
- Hill G., 1982, *Publ. Dom. Astrophys. Obs. Victoria BC*, 16, 67
- Kortenkamp S.J., Malhotra R., Michtchenko T., 2004, *Icarus*, 167, 347
- Levison H.F., Bottke W.F., Gounelle M., Morbidelli A., Nesvorný D., Tsiganis K., 2009, *Nature*, 460, 364
- Levison H.F., Duncan M., 1994, *Icarus*, 108, 18
- Malhotra R., 1995, *AJ*, 110, 420
- Minton D.A., Malhotra R., 2009, *Nature*, 457, 1109
- Morbidelli A., Tsiganis K., Crida A., Levison H.F., Gomes R., 2007, *AJ*, 134, 1790
- Morbidelli A., Brassier R., Tsiganis K., Gomes R., Levison H.F., 2009, *A&A*, 507, 1041
- Morbidelli A., Brassier R., Gomes R., Levison H.F., Tsiganis K., 2010, *AJ*, accepted
- Nesvorný D., Bottke W.F., Levison H.F., Dones L., 2003, *ApJ*, 591, 486
- Nesvorný D., Vokrouhlický D., Morbidelli A. 2007 *AJ*, 133, 1962
- Press W.H., Teukolsky S.A., Vetterlink W.T., Flannery B.P., 1999, *Numerical Recipes in Fortran 77*. Cambridge Univ. Press, Cambridge
- Roig F., Ferraz-Mello S., 1999, *P&SS*, 47, 653
- Roig F., Nesvorný D., Ferraz-Mello S., 2002, *MNRAS*, 335, 417
- Quinn T.R., Tremaine S., Duncan M., 1991, *AJ*, 101, 2287
- Tsiganis K., Gomes R., Morbidelli A., Levison H.F., 2005, *Nature*, 435, 459
- Tsiganis K., Knežević Z., Varvoglis H., 2007, *Icarus*, 186, 484
- Vokrouhlický D., Brož M., Bottke W.F., Nesvorný D., Morbidelli A., 2006a, *Icarus*, 182, 92
- Vokrouhlický D., Brož M., Bottke W.F., Nesvorný D., Morbidelli A., 2006b, *Icarus*, 182, 118
- Zappalà V., Cellino A., Farinella P., Milani A., 1994, *AJ*, 107, 772

This paper has been typeset from a  $\text{\TeX}$ / $\text{\LaTeX}$  file prepared by the author.